FOR GROUND EFFECTS WORKSHOP
NASA AMES RESEARCH CENTER
20 AUGUST 1985

STOL LANDING THRUST - REVERSER JET FLOWFIELDS

D. R. KOTANSKY
L. W. GLAZE
MCDONNELL AIRCRAFT COMPANY
ST. LOUIS, MISSOURI

ABSTRACT

Analysis tools and modeling concepts for jet flowfields encountered upon use of thrust reversers for high performance military aircraft are described. A semi-empirical model of the reverser ground wall-jet interaction with the uniform cross-flow due to aircraft forward velocity is described. This ground interaction model is used to demonstrate exhaust gas ingestion conditions. The effects of control of exhaust jet vector angle, lateral splay, and moving versus fixed ground simulation are discussed. The Adler/Baron jet-in-crossflow model is used in conjunction with three dimensional panel methods to investigate the upper surface jet induced flowfield.

LIST OF SYMBOLS

A	Area
C^2	Freestream momentum correction factor
$C_{yV.T}$	Vertical tail side force coefficient
D	Diameter
f	Wall jet momentum azimuthal distribution function
h, H	Height above ground
M	Mach number
$\dot{m}$	Mass flow rate
NPR	Nozzle pressure ratio
NTR	Nozzle temperature ratio
q	Dynamic pressure
R	Radial distance
$R_{V/2}$	Radial distance in free jet from centerline to the point where the velocity is 1/2 of the centerline value
U_R	Wall jet radial velocity
V	Velocity
x, y, z	Cartesian coordinates
α	Angle of attack
γ	Momentum correction (see Reference 1)
δ_L	Thrust reverser lower vane deflection angle
δ_{je}	Jet injection angle
θ	Stagnation line slope
ρ	Density
ϕ'	Computational azimuth angle
ψ	Freestream-to-jet exit velocity ratio (V_c/V_{je})

Subscripts

c	Cross-flow, freestream
jc	jet centerline
je	jet exit
max	Maximum
min	Minimum
R	Radial
wj	Wall jet

EXHAUST GAS INGESTION

The impingement on the ground of VTOL aircraft lift jet flows in the presence of cross-winds or the impingement of STOL aircraft vectored jets (considering aircraft forward motion) creates a situation related to, but significantly different from the impingement of jets in a static environment. The significant difference is the presence of a mean flow (due to the cross-flow or aircraft motion) which is superimposed on the multiple jet impingement flowfield. The interaction of the mean flow with the existing wall jets and fountains produces a class of turbulent flow interactions which are more complex. Within this class of interactions, there is an additional difference, namely, the effect of forward motion of the aircraft produces a flow without a boundary layer, whereas the cross-flow includes a surface boundary layer. Empirical and analytical tools for the analysis and prediction of the interaction of a mean flow with a single impinging jet will be presented. Specifically, the interaction of a turbulent wall jet with a cross-flow with and without a boundary layer will be addressed. Analysis and prediction of these types of interaction is vital to the prediction of engine exhaust gas ingestion during the landing of a STOL aircraft with thrust reversers.

The ground flowfield associated with thrust reversal in STOL landing is depicted in Figure 1. V_c is the aircraft forward velocity, and δ_L is the thrust vector angle with respect to the aircraft longitudinal axis. In most applications, δ_L is 115° to 150° depending on the aircraft configuration. At high values of V_c, the ground stagnation line is located in the aft region of the aircraft flowfield, but as the aircraft decelerates, the stagnation line moves forward, increasing the potential for exhaust gas ingestion. Since the cross-flow deflects the fountain upwash in an aft direction, a conservative boundary for exhaust gas ingestion is the condition for which the ground stagnation line is located directly below the aft-most portion of the inlet.

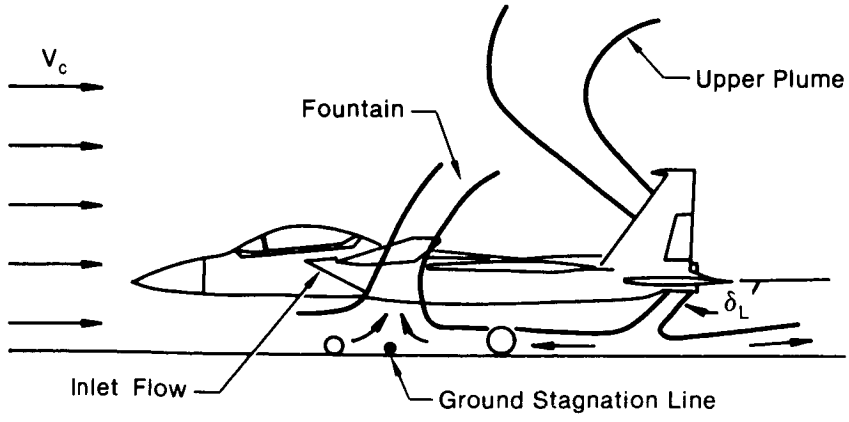

Figure 1. Ground Flowfield With Thrust Reversal

Using this criterion for the potential initiation of exhaust gas ingestion, the problem becomes that of predicting under what condition the ground wall jet stagnation line reaches this location. Additionally, once this condition is reached, for whatever imposed precautionary margin, the problem is to control the flowfield to preclude exhaust ingestion. Methods to achieve this control of jet effects will be discussed later.

The basic relationships for the interaction of a uniform cross-flow with a wall jet emanating from an impinging jet can be derived for an elemental control volume located on the stagnation line. The control volume for this case is shown in Figure 2. Employing a momentum balance normal to the stagnation line for this control volume:

$$\rho V_c^2 \sin\theta \; dy \; dz = \rho U_R^2 \sin(\phi' - \theta) \; R \; \partial\phi' \; dz \tag{1}$$

Integrating Equation (1) to the wall jet height, h, yields:

$$\rho V_c^2 \sin\theta \; h \; dy = \frac{\gamma f \dot{M}_j}{2\pi} \partial\phi' \sin(\phi' - \theta) \tag{2}$$

whereas for an impinging jet (Reference 1):

$$\rho R \; \partial\phi' \int_0^h U_R^2 \, dz = \frac{\gamma f \dot{M}_j}{2\pi} \partial\phi' \tag{3}$$

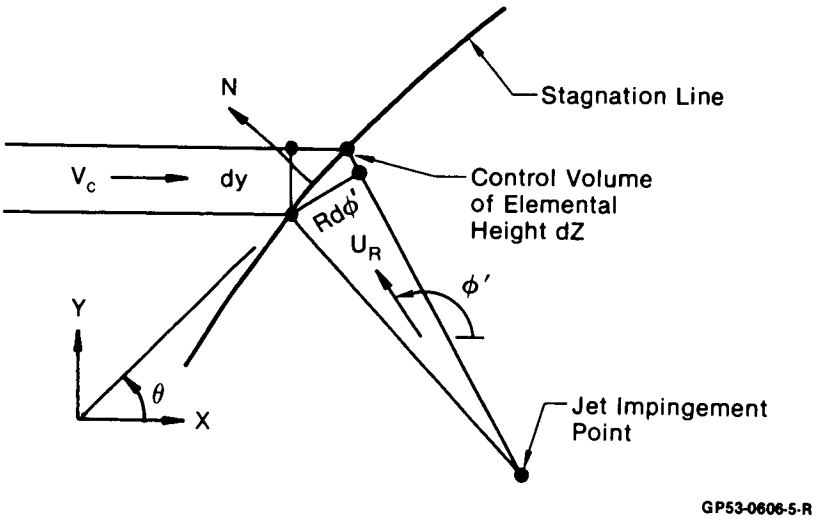

Figure 2. Control Volume for Cross-Flow/Wall-Jet Interaction

To implement the momentum flux density method (MFDM) for $\theta \cong \frac{\pi}{2}$ (see also Reference 2), the left and right hand sides of Equation (2) are divided by their respective momentum flux areas, h dy and h R $\partial\phi'$, yielding:

$$\rho V_c^2 \sin\theta = \frac{\gamma f \dot{M}_j}{2\pi R h} \sin(\phi' - \theta) \tag{4}$$

The above can be solved for the slope of the stagnation line in the ground plane, yielding:

$$\tan \theta = \frac{\beta \sin \phi'}{1 + \beta \cos \phi'} \tag{5}$$

where:

$$\beta = \frac{\gamma f \dot{M}_j}{2\pi R \, h \, \rho V_c^2} \tag{6}$$

For a jet impinging symmetrically with respect to the cross-flow direction, $\phi' = 180°$ and $\theta = 90°$, and the stagnation line distance is given by:

$$R = \frac{\gamma f \dot{M}_j}{2\pi \, h \, \rho V_c^2} \tag{7}$$

However, h is a function of R, and to solve Equation (7) this relationship must be considered. The relationship can be derived from existing wall jet data, and in general, h may be assumed to be a linear function of R. (A slightly more complicated expression for h(R) was derived in Reference 1 based on the data of Reference 3. Either expression yields a quadratic equation which can be solved for R.)

It is instructive to compare the results of the MFDM with those of the momentum flux method, MFM. The MFM result can be derived starting with the fundamental result expressed by Equation (2). Additionally from Figure 3, the following geometric relationships can be obtained:

$$d\ell = \frac{R \, \partial\phi'}{\sin (\phi' - \theta)} = \frac{dy}{\sin\theta} \tag{8}$$

or:

$$\partial\phi' = \frac{\sin (\phi' - \theta)}{R \sin \theta} \, dy$$

Substituting Equation (8) into Equation (2) yields:

$$h \, \rho V_c^2 \sin^2 \theta = \frac{\gamma f \dot{M}_j}{2\pi R} \sin^2 (\phi' - \theta) \tag{9}$$

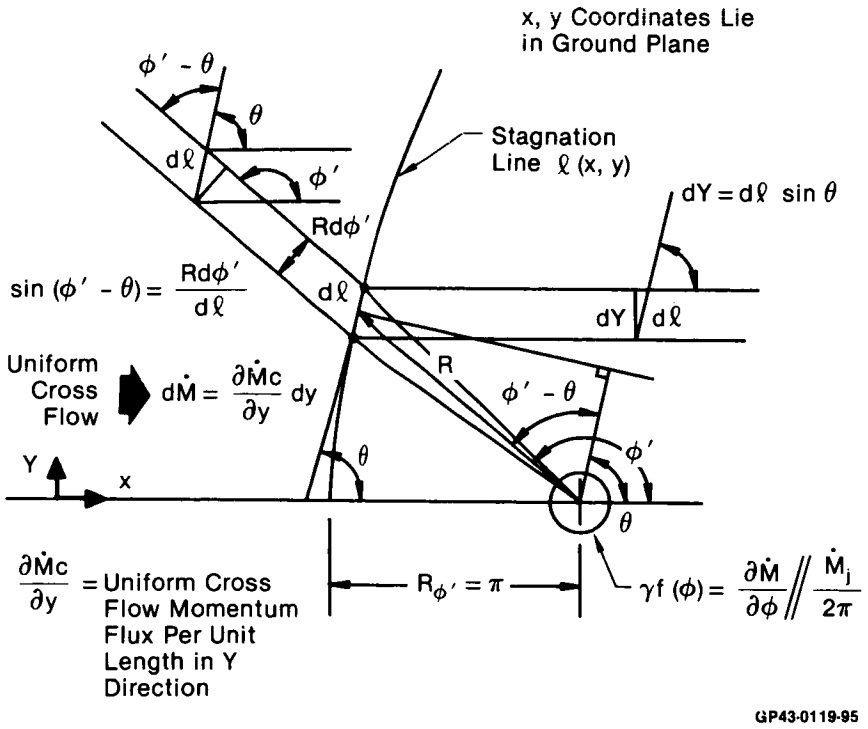

Figure 3. Interaction Geometry - Radial Wall-Jet and Uniform Cross-Flow

This result was first derived in Reference 1, in which the quantity $\frac{\partial \dot{M}_c}{\partial y}$, Figure 3, represented the momentum flux per unit length in the y direction. Equation (9) can be obtained from the results of Reference 1 by selecting:

$$\frac{\partial \dot{M}_c}{\partial y} = \rho V_c^2 h \tag{10}$$

Equations (10) and (2) are based on the assumption that the cross-flow momentum flux per unit length in the y direction need include only that amount contained in an area defined by dy and the height of the interacting wall jet, h. (There is no characteristic height in the uniform cross-flow.)

In the momentum flux method, the slope of the stagnation line in the ground plane can be obtained by solving Equation (9):

$$\tan\theta = \frac{\beta \sin\phi'}{1 + \beta\cos\phi'} \tag{11}$$

where:

$$\beta = \sqrt{\frac{\gamma f \dot{M}_j}{2\pi R \rho V_c^2 h}} \tag{12}$$

For a jet impinging symmetrically with respect to the cross-flow direction, $\phi' = 180°$ and $\theta = 90°$, and the stagnation line distance, from Equation (9), is:

$$R = \frac{\gamma\ f\ \dot{M}_j}{2\pi\ h\ \rho\ V_c^2} \tag{13}$$

which is identical to Equation (7). Therefore, based on the assumption of Equation (10), both the MFDM and the MFM yield the same result for the distance of penetration of the wall jet into the uniform cross-flow.

Comparisons of stagnation line computations based on the stagnation line slope equations, Equations (5) and (6) versus (11) and (12), show very little effect on stagnation line position or shape. Therefore, the MFDM has been incorporated into the MCAIR ground flowfield prediction methodology. The linear relation relating the wall jet height, h, to the radius, R, developed in Reference 1, is also used.

$$h = \sigma_1 + \sigma_2\ R \tag{14}$$

Comparisons of the above results with the experimental data of Reference 4 indicated that an additional empirical correction was required to obtain agreement with the experimental data for wall jet penetration into a uniform cross-flow. The empirical correction is applied to the cross-flow momentum flux per unit length, dy, as given by

$$\frac{\partial \dot{M}_c}{\partial y} = C^2\ \rho V^2\ h \tag{15}$$

Equations (5), (6), and (7) then become:

$$\tan\theta = \frac{\beta\ \sin\phi'}{1 + \beta\cos\ \phi'} \tag{16}$$

where

$$\beta = \frac{\gamma\ f\ \dot{M}_j}{2\pi\ R\ h\ C^2\ \rho V_c^2} \tag{17}$$

and

$$R = \frac{\gamma\ f\ \dot{M}_j}{2\ \pi h\ C^2\ \rho\ V_c^2} \tag{18}$$

The values of C^2 for wall jet penetration into uniform cross-flows and for cross-flows with boundary layers was determined from References 4 and 5 respectively.

In Reference 4, the penetration of a single impinging jet into a uniform cross-flow was studied for both hot and ambient temperature jets. The uniform cross-flow interaction was simulated by moving the impinging jet through ambient air, supporting it on a rotary support system. Except for minor centrifugal effects, this test technique correctly simulates the STOL jet impingement situation, including the retardation of the wall jet due to the relative motion of the nozzle along the fixed ground plane. The correct simulation can be obtained in a conventional wind tunnel only through the use of a moving ground plane. The correlation of penetration distance into the cross-flow is shown in Figure 4, taken from Reference 4. The geometry and nomenclature are defined in Figure 5.

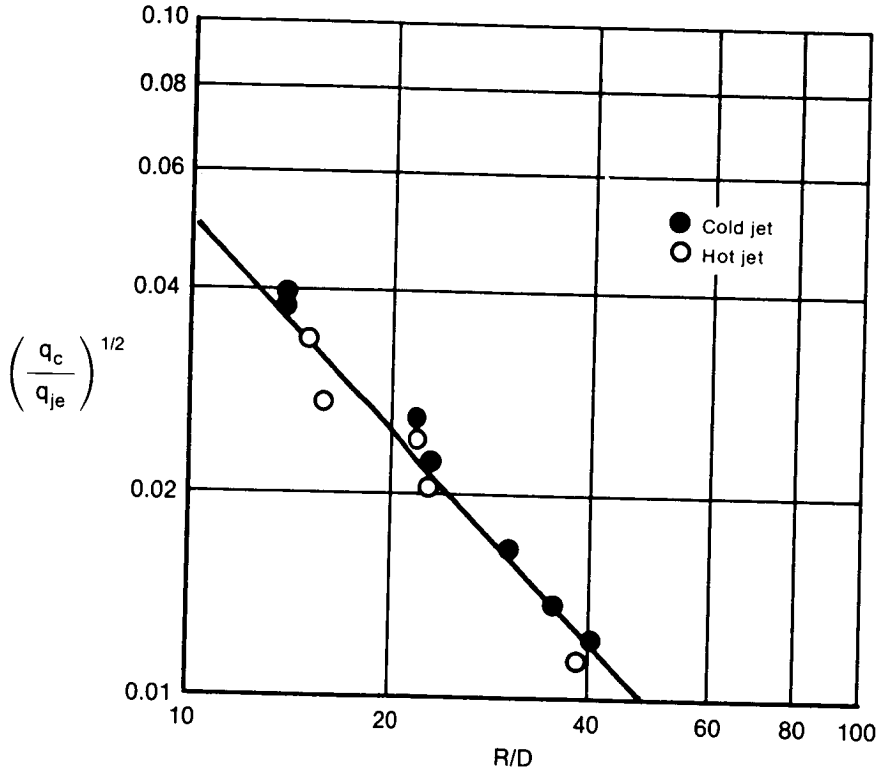

Figure 4. Jet Penetration Into Uniform Cross-Flow for Hot and Cold Jets

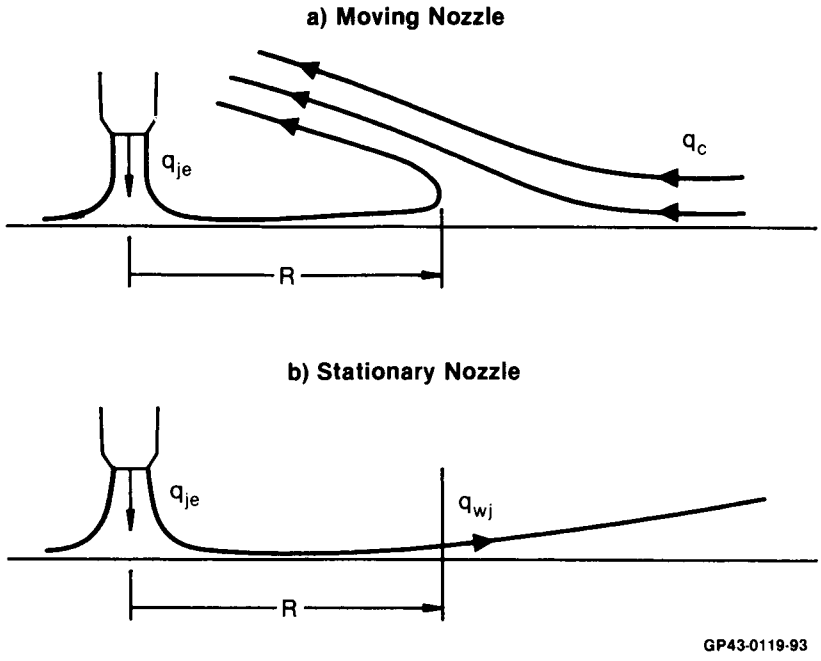

Figure 5. Jet Penetration Nomenclature

Another empirical correlation from Reference 4 shows that:

$$(q_c/q_{wj})^{1/2} \cong 0.5 \tag{19}$$

which indicates, from Figure 5, that the stagnation line in the cross-flow situation occurs at a distance corresponding to the static jet impingement situation where:

$$q_{wj} \cong 4\, q_c \tag{20}$$

In other words, the wall jet penetrates into the cross-flow much less than would be expected from an equivalence of local dynamic pressures. This can be accounted for in the analytical models by artificially increasing the cross-flow momentum as shown in Equation (15).

From Reference 4 it can be expected that $C^2 = 4$ for the uniform cross-flow case without a cross-flow boundary layer. Equations (16), (17), and (18) were used to determine the value of C^2 to fit the data correlation of Reference 4, shown in Figure 4. The empirically determined value of C^2 was found to be:

$$C^2_{\text{uniform cross-flow}} = 3.61 \tag{21}$$

This value of C^2 is used in the MCAIR ground flowfield methodology for the uniform cross-flow interaction with no cross-flow boundary layer and where the wall jet is retarded by the relative motion of the ground plane. The interaction with and without a moving ground plane is shown in Figure 6. With a fixed ground plane, the jet impinges statically, and the cross-flow includes a boundary layer. In the moving ground plane situation which simulates a STOL landing, the stagnation line shifts aft due to the lack of a boundary layer in the cross-flow and due to the retardation of the wall jet.

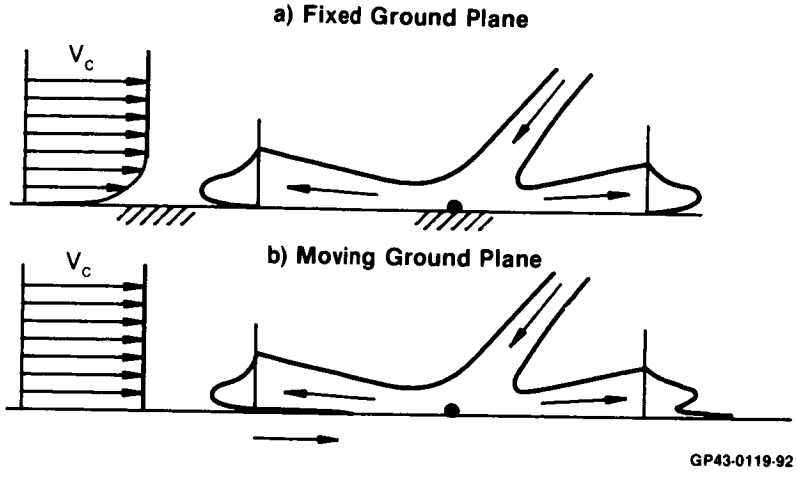

Figure 6. Fixed vs Moving Ground Plane Interactions

In the case of a fixed ground plane, Figure 6a, C^2 would be expected to be less than the value of 3.61 obtained for the moving ground plane case. The data of Reference 5 was used to determine C^2 for this situation. This data is correlated analytically as:

$$\frac{R}{D} = 0.61\left(\frac{q_{je}}{q_c}\right)^{1/2} \tag{22}$$

The data correlated by Equation (22) also included variations in nozzle exit flow temperature.

For this situation, the correlating value of C^2 for use in the MCAIR ground flowfield methodology was determined to be:

$$C^2_{\text{fixed ground plane}} = 2.40 \tag{23}$$

These correlations are summarized in Figure 7, where the variation of the wall jet stagnation line or separation distance is shown as a function of the dynamic pressure ratio between the nozzle exit and the cross-flow. The curve labeled "Uncorrected MFDM" corresponds to $C^2 = 1.0$, which usually overpredicts the penetration of the wall jet into the cross-flow. The correlations corresponding to the moving ground and fixed ground plane situations were obtained using the values of C^2 given in Equations (21) and (23), respectively, based on the data of References 4 and 5. Shown also in Figure 7 are data correlations for two values of H/D from wind tunnel and moving ground vehicle tests of ingestion boundaries for the Concorde aircraft configuration with $\delta_L = 115°$. These correlations contain both fixed and moving ground data (Reference 6).

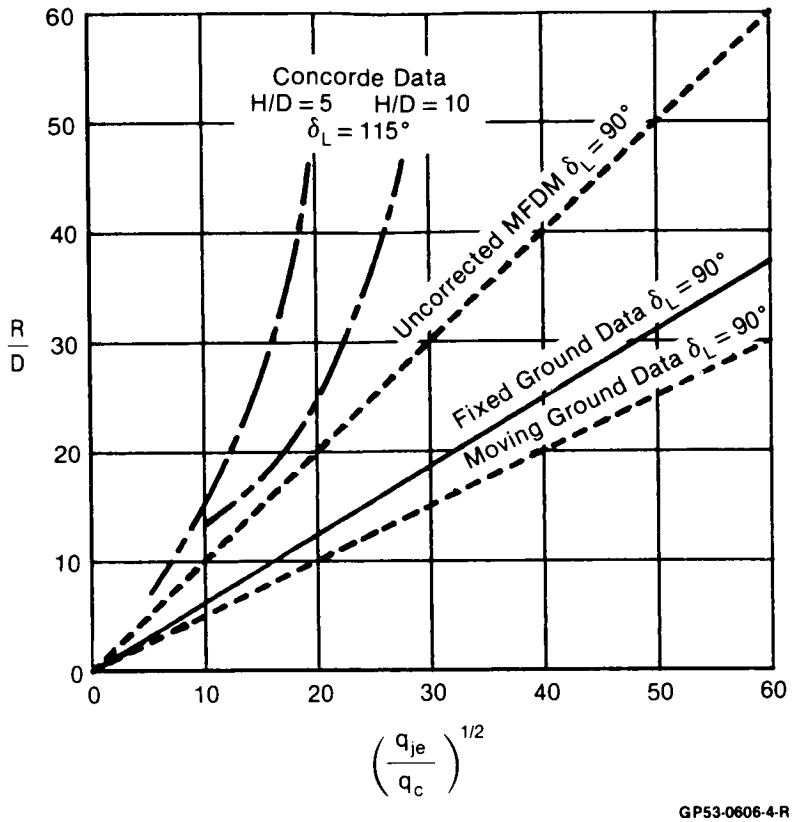

Figure 7. Correlation of Wall-Jet Penetration Results - Cross-Flow/Wall-Jet Interaction

To further validate the above computational model, MCAIR determined the value of C^2 that most closely matched a lower surface exhaust deflection schedule developed from two experimental data correlations and a MCAIR empirical technique. The data correlations used were developed for a high performance aircraft during STOL landing ground deceleration and were valid for fixed ground plane simulations. A value of C^2 of 2.50 was found to satisfactorily match the data correlations. This compares well with the previously determined value of 2.40 (Equation 23).

Additional useful information on the effects of fixed versus moving ground plane testing can be found, for example, in References 7 and 8. Reference 8 contains an extensive list of earlier work. Figure 8, taken from Reference 7, substantiates the results presented in Figure 7 in terms of the thrust reverser shown in the figure, which included forward vectoring for reverse thrust plus outboard splay of the reverser jets. It is seen from the figure that the rollout speed for ingestion with the moving ground plane simulation was approximately 15% less than for a fixed ground plane. The effect of NPR is also indicated for this reverser configuration, and in general indicates the expected trends with forward vectored reverser jet impingement for a wide range of configurations. The differences between moving and fixed ground plane simulations may not appear to be large; however, the desired landing rollout distance goals are quite short compared to CTOL high speed aircraft landing distances, and these differences may be critical.

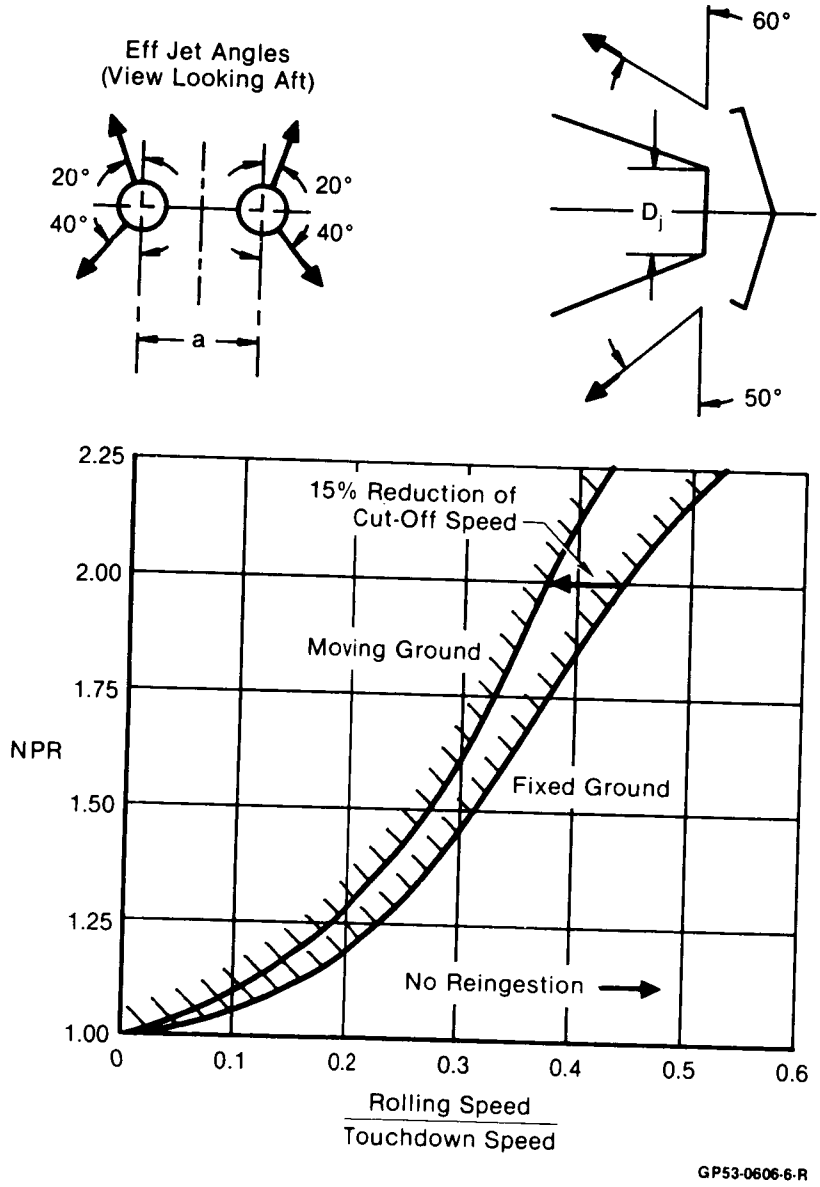

Figure 8. Thrust Reverser Operation Boundary Due to Ingestion for Fixed and Moving Ground Plane Simulations

An alternate empirical method is also used by MCAIR to predict the exhaust gas ingestion potential for STOL aircraft employing thrust reversers during landing rollout. This method is based on the balance of local dynamic pressure in the turbulent wall jet with the dynamic pressure of the cross-flow. A typical decay in the dynamic pressure of a wall jet with increased radius is shown in Figure 9. These data also include cases with elevated nozzle exit flow temperatures.

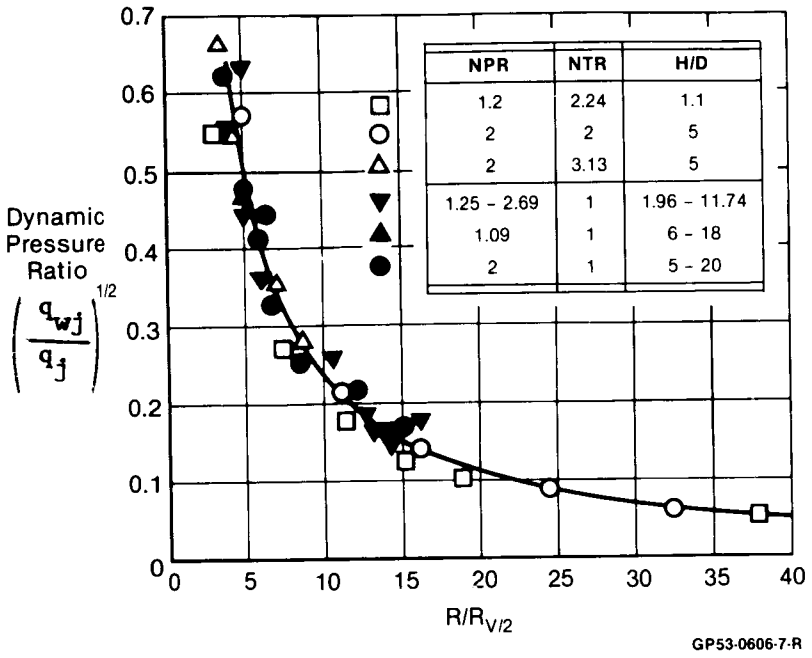

Figure 9. Dynamic Pressure vs Radial Position - Vertical Impingement

Here, q_j is the free jet dynamic pressure locally at the distance down the jet corresponding to the distance from the nozzle exit to the jet impingement point. $R_{v/2}$ is also determined from the free jet velocity profile at this point.

In the fixed ground plane situation, the location of the stagnation line is taken to be at the point where:

$$q_c = q_{wj} \Big|_{\text{average}} = 0.457\, q_{wj} \Big|_{\text{max}} \tag{24}$$

Equation (24) is also used in the moving ground plane situation, but, the cross-flow dynamic pressure is multiplied by a factor of four; i.e.,

$$q_c \Big|_{\text{moving ground}} = 4\, q_c \tag{25}$$

which relates to Equation (20) based on the data of Reference 4.

Figure 10 presents computations of the ground stagnation line for a typical high speed fighter employing thrust reversers. Stagnation line locations predicted by the MCAIR empirical method are shown as a function of aircraft ground roll speed (headwind velocity) for thrust reversal with and without lateral splay. The beneficial effect of splay is apparent; however, a component of reverse thrust can be lost if the splay is not obtained through a rotation of the reverser about the aircraft longitudinal axis.

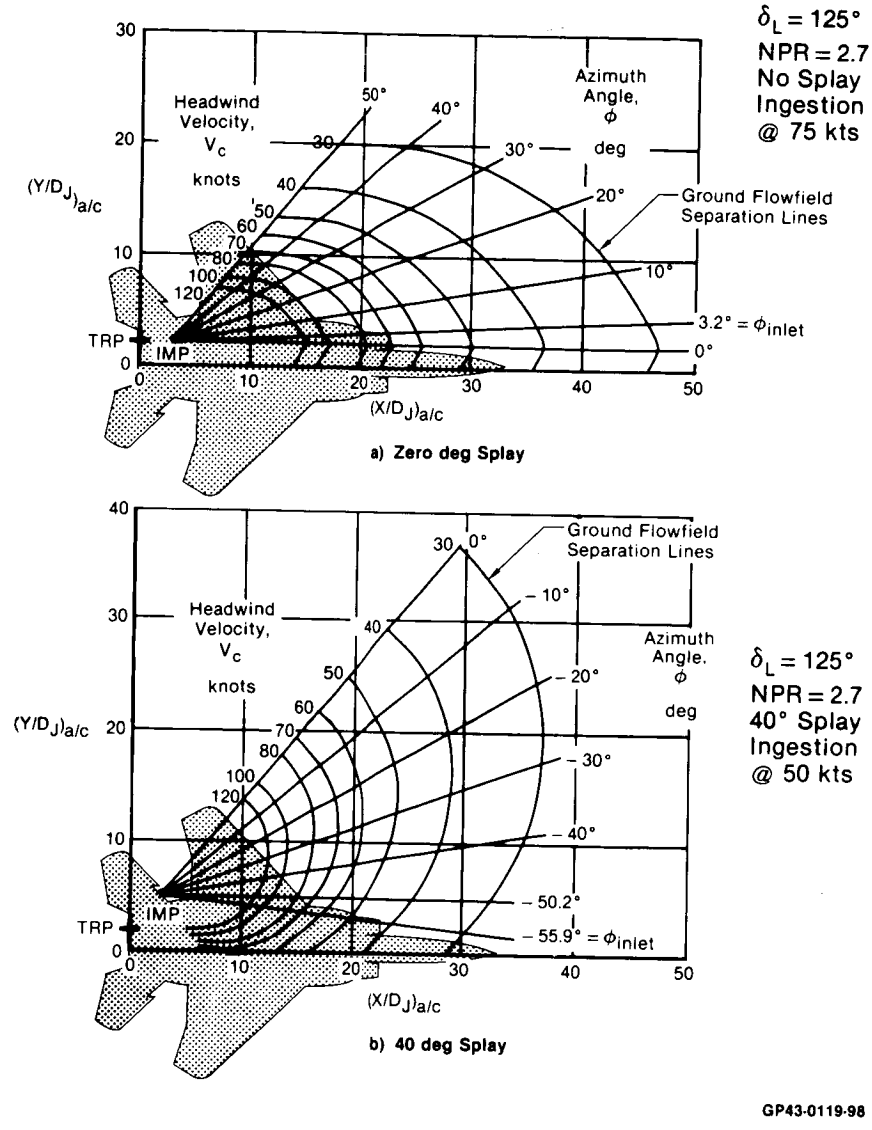

Figure 10. MCAIR Empirical Method Ground Separation Line Predictions

Exhaust gas ingestion can be reduced, and in fact eliminated, on ground rollout through thoughtful configuration design, and, additionally, through active control of the direction of jet efflux. Thrust reverser designs employing variable vectoring vanes can be used to direct the jet efflux to maintain the ground stagnation line aft of the aircraft inlet as the rollout velocity is reduced, while still providing significant reverse thrust. These systems, combined with conventional mechanical wheel braking, can provide excellent STOL landing performance.

UPPER SURFACE JET FLOWFIELD

The jet efflux from upper surface thrust reversers can considerably alter the aircraft upper surface flowfield. Elements of concern include:

- Effects on tail mechanical loads,
- Changes in stability and control characteristics in ground effect,
- Aircraft surface temperatures.

Some features of the upper surface flowfield can be predicted by panel methods such as PANAIR or MCAERO, used in conjunction with a suitable jet-in-cross-flow model. The following will describe the jet-in-cross-flow model used at MCAIR.

The MCAIR V/STOL Methodology currently derives information on jets emanating from circular (or nearly circular) nozzles from the Adler-Baron Jet-In-Cross-Flow program, JICP, (Reference 9). The basic method was developed for incompressible jets submerged in a uniform cross-flow. The jet injection angle, δ_{je}, and freestream-to-jet-exit velocity ratio, ψ, are variable over a useful range. (MCAIR has modified the basic Adler-Baron formulation to include some non-circular jet exit shapes, and also to permit forward jet injection angles, for analysis of thrust reverser flowfields).

A schematic of jet-in-cross-flow development is shown in Figure 11. The jet is deflected downstream by the momentum of the cross-flow. As the jet develops downstream, the vorticity generated by the basic jet injection, combined with the flow of the cross-flow around the jet, forms a pair of contrarotating vortices which tend to dominate the downstream development of the jet. Induced flowfield velocities result from:

(a) the basic blockage of the jet,
(b) the turbulent entrainment (similar to a free jet), and
(c) vortex induction.

In general, the centerlines of the vortices lie above the nominal jet centerline. Trajectories of both the jet centerline and the vortex centerlines are given in Reference 10 for round jets.

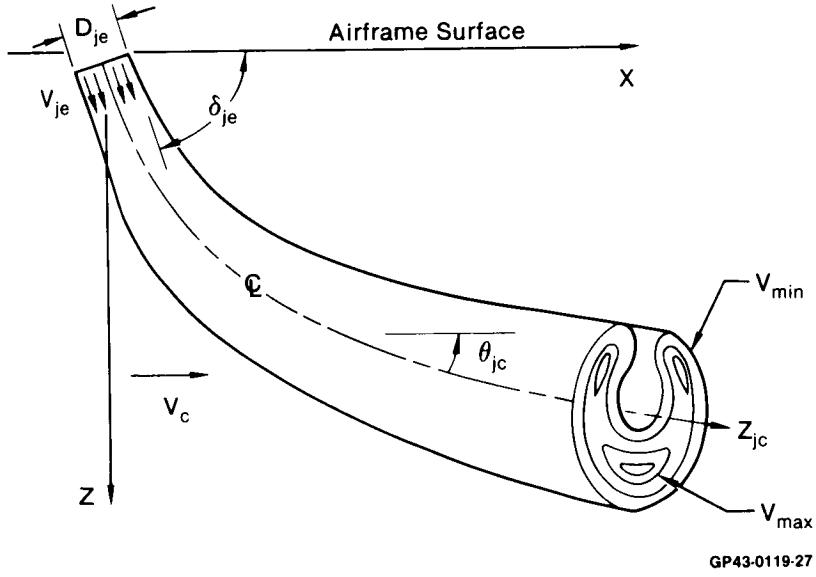

Figure 11. Jet-In-Crossflow at High Injection Angle

The basic Adler-Baron model (Reference 9) incorporates some simplifying assumptions, namely: 1) external flowfield is irrotational; 2) the mixing field is isothermal and of uniform composition (no heat transfer or diffusion); 3) the flow is turbulent; 4) the flow is incompressible and steady; 5) the jet centerline is defined as the locus of the momentum centers of cross sections; 6) velocities are parallel to the centerline; 7) cross-section boundary of the jet is the locus of points at which the velocity excess in the direction of the centerline vanishes (or is smaller than a prescribed small value); 8) pressure on cross sections is uniform and proportional to $V_c \cos\theta_{jc}$; 9) most of the entrainment takes place in the vortex pair tail.

A control volume in the jet is used to derive the governing two momentum equations of the integral model. These two integral momentum equations, together with four additional equations - i.e., the expansion rate equation, the shape equations, and the normalized velocity profile equation - describe the jet mixing field completely.

Two momentum equations are developed: one parallel to the jet centerline and one perpendicular to it. The momentum balance includes entrained momentum, surface forces on the jet (drag force) and centrifugal body forces. To complete the formulation, one must determine the rate of the jet growth, the shape of the cross sections, and the velocity profiles. t is assumed that the jet cross-section area growth is a linear superposition of two growing mechanisms: 1) growth of a straight turbulent jet in a quiescent environment; and 2) growth of a vortex pair (in accordance with Assumption 9). Although this model of jet growth seems to be an over-simplification, it yields acceptable results.

The cross-section shape calculation predicts approximately the development of the geometry (but not the areas) of these shapes from a circle into the developed horseshoe configuration. This shape development contains much of the nonsimilarity of the mixing process, so that its prediction is essential for a representative model. The cross-section distortion is determined by evenly seeding a finite number of vortices, N, on the instantaneous boundary of the jet and calculating their displacement over a small time period due to their induced velocity. The induced velocity components of each vortex are calculated, and the vortices are displaced accordingly, as the computation progresses down the jet.

The internal jet velocity profiles are obtained from a solution of Poisson's equation within the jet cross-section, combined with empirical parameters.

The Jet-In-Cross-Flow Program is restricted to one isolated jet issuing from a flat plate into the freestream. Due to the weak effect of the airframe on the jet, it is reasonable to calculate the jet properties in isolation. For multiple jets, the program is executed once for each jet. For tandem jets, as is the case for the YAV-8B, the upstream jet exerts a large influence on the downstream one, and the jets tend to coalesce. The method of Wooler (Reference 11) is used to determine the blockage effects of the upstream jet on the downstream jet. The merged single jet properties are determined to a first order approximation by simply combining the effects of the individual jets without coalescence.

The accuracy of the Adler-Baron JICP is shown in Figures 12-15, where the predicted jet centerline trajectory, cross-sectional area ratio, entrained mass flux, and jet velocity profiles are compared with experimental data, (Reference 12). For the cases examined, the agreement is good. MCAIR extensions of the Adler-Baron JICP for upstream jet injection are shown in Figure 16.

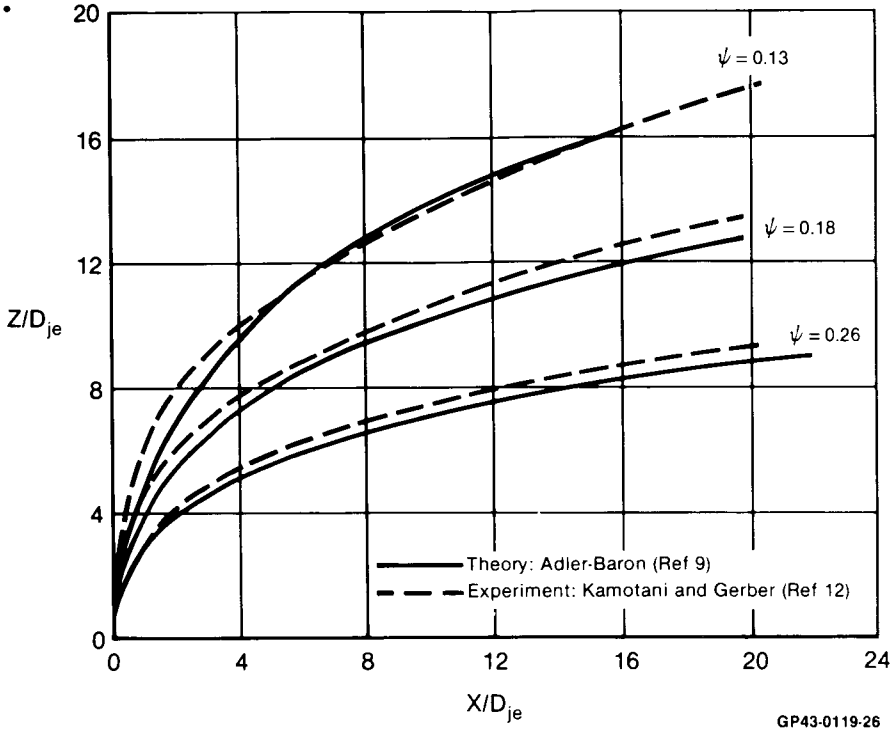

Figure 12. Locus of Peak Jet Velocity Centerline Trajectory
90° Injection Angle

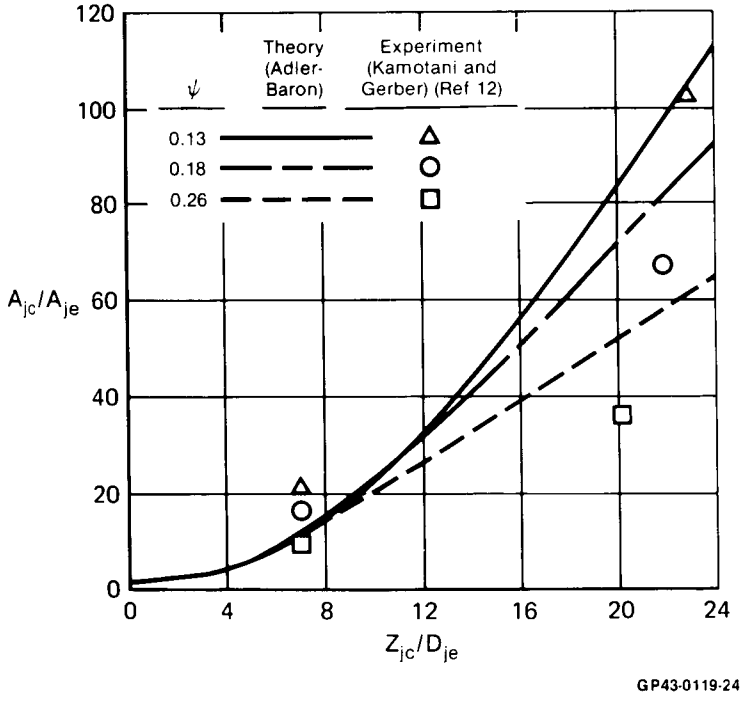

Figure 13. Jet Cross-Sectional Area Ratio Comparison
90° Injection Angle

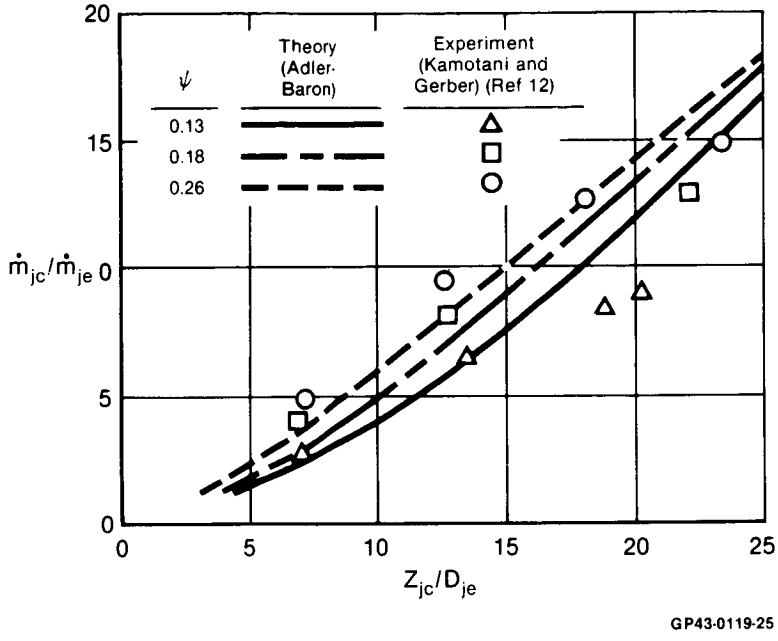

Figure 14. Entrained Mass Flux Comparison
90° Injection Angle

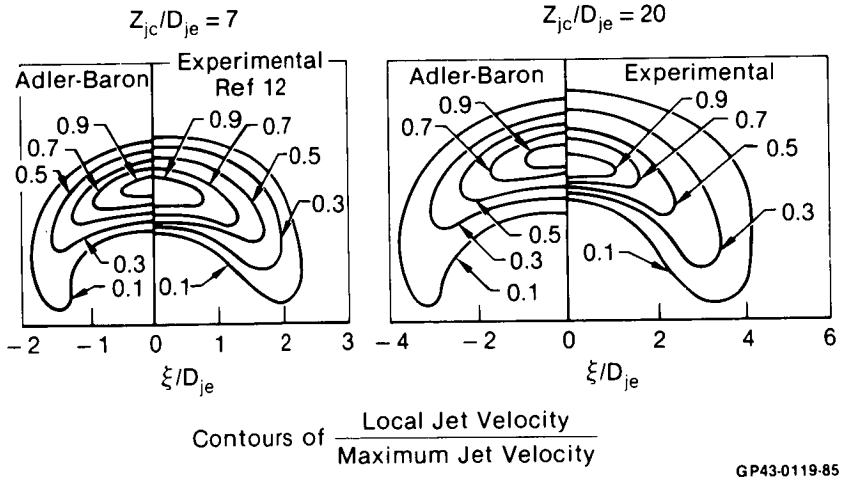

Figure 15. Jet Velocity Profile Comparison
90° Injection Angle $\psi = 0.26$

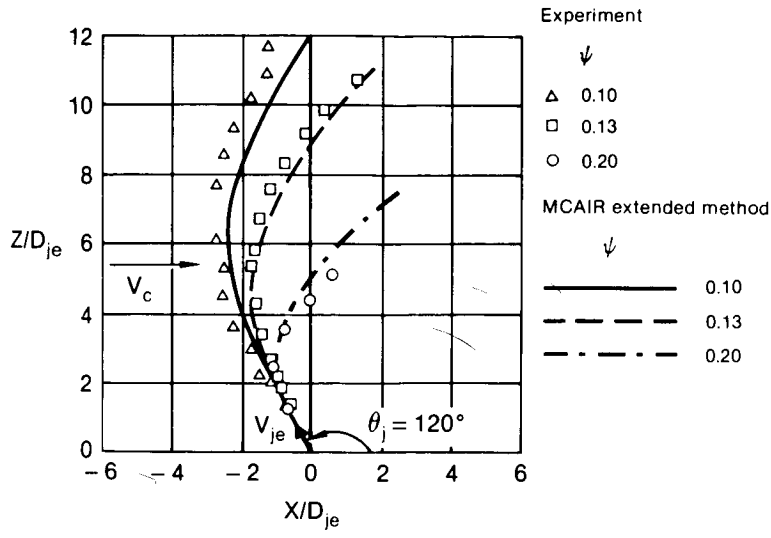

Figure 16. Peak Jet Velocity Centerline Trajectory for Jet Injection Against the Freestream

The MCAIR V/STOL methodology requires the jet-in-cross-flow characteristics obtained from the Adler-Baron JICP to be modelled in the MCAIR three-dimensional Subsonic Potential Flow Program. Figure 17 demonstrates the panelling model of the jet in cross-flow. The three-dimensional outer surface of the jet is obtained from the JICP. The "windward" side of the jet is panelled as a solid surface which models the blockage effect of the jet in cross-flow. The "leeward" side of the jet (shaded panels in Figure 17) is made up of panels with a prescribed distribution of normal velocities to simulate the entrainment and velocity distribution induced by the jet-in-cross-flow vortex structure.

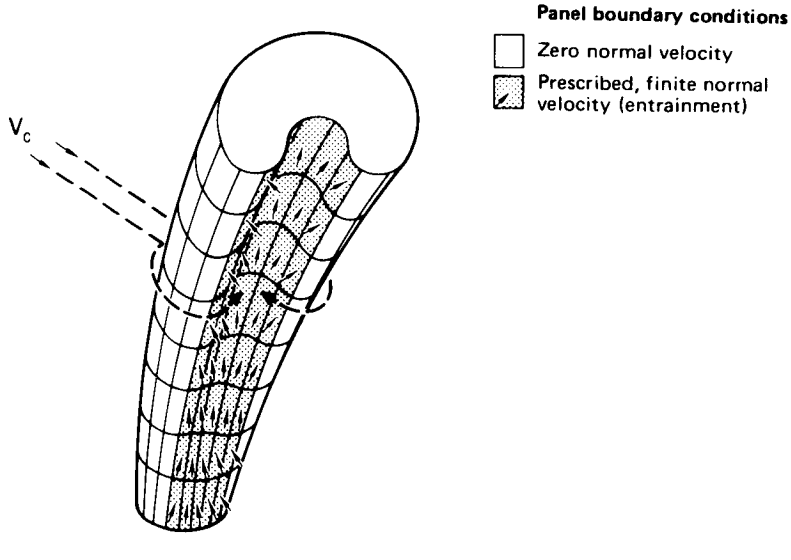

Figure 17. Paneled Representation of a Jet-In-Crossflow

To illustrate an application of the MCAIR jet-in-cross flow methodology to predict the effects of an upper surface jet flowfield, the blockage effects of a single thrust reverser jet on twin vertical tail loads were calculated. The analysis was performed for a thrust reverser jet injection angle (δ_{je}) of 135° and a freestream-to-jet velocity ratio (ψ) of .073. The thrust reverser jet trajectory and geometry were determined using the Adler-Baron Jet-in-Cross-Flow program, and the vertical tail loads and pressure distributions were calculated using MCAERO. Since only the local vertical tail flowfield was of interest, only the fuselage, vertical tails and jet were modeled. The jet exit was circular with an area equivalent to that of current twin reverser configurations.

The MCAERO analyses were performed both with and without the jet for $M = 0.2$ and $\alpha = 0°$. A vertical tail side force coefficient, $C_{y_{V.T.}}$, was calculated for each configuration (where $C_{y_{V.T.}}$ is based on the projected area of a single tail; positive outboard).

The analyses predicted a negative (inboard) side force on the vertical tails, both with and without the jet. However, with the jet, $C_{y_{V.T.}}$ was over 6 times greater than without the jet. The vertical tail chordwise pressure distributions calculated at the 35% span station illustrated increased suction on the inboard side of the tail. This indicated that the jet blockage produced a venturi effect, accelerating the flow over the inboard surface of the tails. The local angle of attack of the vertical tails was changed also, with the flow becoming more inboard with the jet on.

It should be re-emmphasized that this analysis represented the blockage effects of the jet only; no attempt was made to model the jet entrainment. However, specification of entrainment velocities on the paneled jet model would be expected to further reduce $C_{y_{V.T.}}$.

These results apply only to the case presented and may differ qualitatively as well as quantitatively with variations in jet injection angle or velocity ratio.

REFERENCES

1. Kotansky, D. R.; Durando, N. A.; Bristow, D. R.; and Saunders, P. W., "Multi Jet Induced Forces and Moments on VTOL Aircraft Hovering In and Out of Ground Effect," Final Technical Report, NADC Report 77-229-30, June 1977.

2. Kotansky, D. R., "Jet Flowfields," Paper No. 7, Special Course on V/STOL Aerodynamics, AGARD Report No. 710, April, 1984.

3. Donaldson, C. du P., and Snedeker, R. S., "A Study of Free Jet Impingement, Part I - Mean Properties of Free and Impinging Jets," Journal of Fluid Mechanics, Vol. 45, Part 2, pp 281-319, 1971.

4. Abbott, W. A., "Studies of Flow Fields Created by Vertical and Inclined Jets when Stationary or Moving Over a Horizontal Surface," Aeronautical Research Council Current Paper No. 911, Great Britain, October, 1964.

5. Weber, H. A., and Gay, A., "VTOL Reingestion Model Testing of Fountain Control and Wind Effects," AIAA Paper 75-1217, Anaheim, CA, September, 1975.

6. Willmer, A. C., and Scotland, P. L., "Reverse Thrust Experience on the Concorde," AGARD-CP-150, March, 1975.

7. Lotter, K., and Kurz, W., "Aerodynamic Aspects and Optimization of Thrust Reverser Systems," AGARD-CP-150, March, 1975.

8. Margason, R. J., "Jet V/STOL Wind Tunnel Simulation and Ground Plane Effects," AGARD-CP-308, January, 1982.

9. Adler, D., and Baron, A., "Prediction of a Three-Dimensional Circular Turbulent Jet-in-Cross-Flow," AIAA Journal, Vol. 17, No. 2, pp 168-174, February 1979.

10. Fearn, R., and Weston, R. P., "Vorticity Associated with a Jet in Cross-flow," AIAA Journal, Vol. 12, No. 12, December, 1974.

11. Wooler, P. J., "Development of an Analytical Model for the Flow of a Jet into a Subsonic Crosswind," NASA SP-218, September, 1969.

12. Kamotani, Y., and Greber, V., "Experiments on a Turbulent Jet-in-a-Cross-Flow," NASA CR-72893, June, 1971.